Floquet Higher-Order Topological Insulators with Anomalous Dynamical Polarization

Biao Huang[1,*] and W. Vincent Liu[1,2,3,4,†]
[1]Department of Physics and Astronomy, University of Pittsburgh, Pittsburgh PA 15260, USA
[2]Wilczek Quantum Center, School of Physics and Astronomy and T. D. Lee Institute, Shanghai Jiao Tong University, Shanghai 200240, China
[3]Shenzhen Institute for Quantum Science and Engineering and Department of Physics, Southern University of Science and Technology, Shenzhen 518055, China
[4]Shanghai Research Center for Quantum Sciences, Shanghai 201315, China

(Received 17 November 2018; accepted 11 May 2020; published 28 May 2020)

Higher-order topological insulators (HOTIs) have emerged as a new class of phases, whose robust in-gap "corner" modes arise from the bulk higher-order multipoles beyond the dipoles in conventional topological insulators. Here, we incorporate Floquet driving into HOTIs, and report for the first time a dynamical polarization theory with anomalous nonequilibrium multipoles. Further, a proposal to detect not only corner states but also their dynamical origin in cold atoms is demonstrated, with the latter one never achieved before. Experimental determination of anomalous Floquet corner modes is also proposed.

DOI: 10.1103/PhysRevLett.124.216601

Introduction.—Highly nonequilibrium systems challenged our understanding of many-body physics recently. The two cornerstones—spontaneous symmetry breaking and topology—both witnessed major conceptual revolution as time is introduced to play unexpected essential roles. Novel examples include the Floquet time crystals [1–11] with broken time-translation symmetry enforced by spectral pairing [12] rather than the usual energetics. Also, periodic-driven systems support "anomalous" edge states, whose topological origin transcends any description by effective Hamiltonians [13–21].

Meanwhile, rapid progress in cold atom experiments is made regarding dynamical controls [22,23]. High tunability of lattice quench not only reveals fundamental quantities like momentum resolved Berry curvature [24,25] and Wilson lines [26] inaccessible before, but also introduces new topological objects such as Bloch-wave dynamical vortices characterized by spacetime linking number [27–30]. More recently, the advent of quantum gas microscopes further enables dressing and probing with single-site accuracy [31–34].

Inspired by the development, we explore a new class of nonequilibrium phase dubbed the Floquet higher-order topological insulators (FHOTIs), and expose its unique signatures accessible via latest technologies. Here, "higher order" refers to the Bloch-wave multipole polarization compared with dipole ones in conventional topological insulators, resulting in unusual corner or hinge states with reduced dimensionality. Soon after the pioneering works [35,36], extensive experimental breakthroughs [37–42] and theoretical generalizations [43–63] have emerged [64]. Yet, research is stuck on static cases as the concept of "dynamical multipoles" still awaits definition. Also, it is nontrivial to prove experimentally not only the existence but also the dynamical origin of corner or hinge states, with the latter one never achieved before.

This Letter addresses three critical problems to initiate research on FHOTIs. (1) A highly solvable model with rich and analytically obtainable phase diagram is constructed. It serves as a direct experimental blueprint in multiple platforms. (2) The theory of anomalous dynamical polarization is obtained for the first time, featuring both conceptual and phenomenological differences from static ones. (3) Combining microscope and band-tomography techniques, we design the experimental scheme to conclusively prove both the existence of corner states and triviality of Floquet operators. Theoretically, these results pave the way to incorporating dynamical multipoles to, for instance, quantum spin liquids [65], Floquet symmetry protected topological phases [19–21], and holographic Floquet matters in topological semimetals and superconductors [66–68]. Experimentally, our detection scheme in cold atoms may help realize the long-sought goal of distinguishing dynamical boundary states from static ones. Recently, deep connections have developed between Floquet phases and other central issues, including localization [19,69–73] and quantum computations with dynamical Majorana modes [74–76]. Introducing multipole features into Floquet physics would surely add a new dimension to phenomena of intrinsically nonequilibrium nature.

Models and the limitation of static polarization.—Consider the binary Floquet drive $H(\boldsymbol{k}, t+T) = H(\boldsymbol{k}, t)$ in Fig. 1, where

$$H(\boldsymbol{k},t) = \begin{cases} \gamma' h_1, & t \in [0, T/4]; \\ \lambda' h_{2\boldsymbol{k}}, & t \in (T/4, 3T/4]; \\ \gamma' h_1, & t \in (3T/4, T]. \end{cases} \tag{1}$$

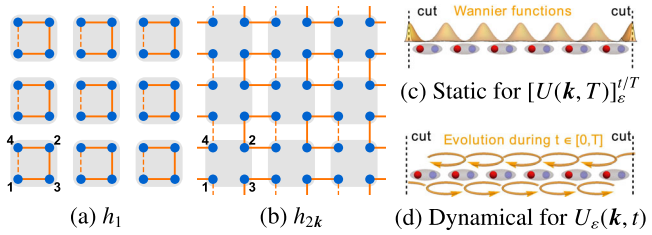

FIG. 1. Connected tetramers during periodic drive at (a) steps 1, 3 and (b) step 2. Solid (dashed) lines represent positive (negative) signs for the hopping with homogeneous magnitudes. (c) Static versus (d) dynamical polarizations.

Here, time origin is shifted to make it transparent $H(\boldsymbol{k},t)=H(\boldsymbol{k},-t)$, and γ',λ' are hopping constants. The system is controlled by dimensionless numbers $(\gamma,\lambda)\equiv(\gamma' T/2\hbar,\lambda' T/2\hbar)$, and all energy (or time) carry units $2\hbar/T$ (or $T/2$). The matrices $h_1=\tau_1\sigma_0-\tau_2\sigma_2$, and $h_{2\boldsymbol{k}}=\cos k_x\tau_1\sigma_0-\sin k_x\tau_2\sigma_3-\cos k_y\tau_2\sigma_2-\sin k_y\tau_2\sigma_1$, where $\boldsymbol{\tau}$, $\boldsymbol{\sigma}$ are Pauli matrices spanning the basis for four sublattices $(\hat{c}_{\boldsymbol{k}1},\hat{c}_{\boldsymbol{k}2},\hat{c}_{\boldsymbol{k}3},\hat{c}_{\boldsymbol{k}4})^T$ [77]. Then, the evolution operator $U(\boldsymbol{k},t)=P_\tau e^{-(i/\hbar)\int_0^t H(\boldsymbol{k},\tau)d\tau}$, with P_τ time ordering. Such a tetramer model enjoys high solvability and rich phase diagrams, as we shall see.

"Anomalous" and "normal" Floquet physics can be separated by decomposing [13–15]

$$U(\boldsymbol{k},t)=U_\varepsilon(\boldsymbol{k},t)[U(\boldsymbol{k},T)]_\varepsilon^{t/T}. \tag{2}$$

Here, the normal part $[U(\boldsymbol{k},T)]_\varepsilon^{t/T}$ takes the t/T exponential with branch cut ε, $(e^{iE_{\alpha\boldsymbol{k}}})_\varepsilon^{t/T}$ on eigenvalues of the Floquet operator $[U(\boldsymbol{k},T)]_{mn}=\sum_\alpha[u_{\alpha,\boldsymbol{k}}]_m e^{iE_{\alpha\boldsymbol{k}}}[u_{\alpha,\boldsymbol{k}}]_n^*$. m, n (or α) $=1,\ldots,4$ are sublattice (or band) indices. With accumulative band physics factored out to $[U(\boldsymbol{k},T)]_\varepsilon^{t/T}$, the periodic part $U_\varepsilon(\boldsymbol{k},t+T)=U_\varepsilon(\boldsymbol{k},t)$ describes anomalous Floquet topology from purely dynamical processes. Choosing ε in a certain bulk gap for $U(\boldsymbol{k},T)$ means investigating possible in-gap open-boundary states resulting from $U_\varepsilon(\boldsymbol{k},t)$.

Higher-order polarization theory lies at the heart and gives rise to the name "higher-order" topological insulators. Thus, it is worth reviewing its conventional static version [35] to understand the limitations. Static polarization focuses on position operators projected to occupied *bands* α, $\hat{y}_{\rm occ}=\hat{P}_{\rm occ}\hat{y}\hat{P}_{\rm occ}$, where $\hat{P}_{\rm occ}=\sum_{\alpha=1}^{N_{\rm occ}}\hat{\gamma}_{\alpha\boldsymbol{k}}^\dagger|0\rangle\langle 0|\hat{\gamma}_{\alpha\boldsymbol{k}}$ are projectors with $\hat{\gamma}_{\alpha\boldsymbol{k}}^\dagger=\sum_m[u_{\alpha\boldsymbol{k}}]_m\hat{c}_{\boldsymbol{k}m}^\dagger$ band creation operators. $\hat{y}=\sum_{im}\hat{c}_{im}^\dagger|0\rangle e^{-i\Delta_{y}y_i}\langle 0|\hat{c}_{im}$ is Resta's [78] position operator satisfying the periodic boundary condition, with $i=(x_i,y_i)$ denoting unit cells on $L_x\times L_y$ lattices, and $\Delta_y=2\pi/L_y$. Essential physics is that collective (Wannier) wave functions in the occupied bands may be polarized away from unit cells by ν_j and center in between, as illustrated in Fig. 1(c). This is captured by the eigenvalues of $\hat{y}_{\rm occ}=\sum_{j,y_i}|w_j(y_i)\rangle e^{-i\Delta_y(y_i+\nu_j)}\langle w_j(y_i)|$, compared with $e^{-i\Delta_y y_i}$ for $\hat{y}$. The static polarization in semi-infinite samples is then $p_y(x_i)=(2\pi L_y)^{-1}\sum_{jy_ik_ym}|\langle 0|\hat{c}_{k_y,mx_i}|w_j(y_i)\rangle|^2\nu_j$ (see Supplemental Material [79] for computation details).

Clearly, the very definition of static polarization necessarily involves (quasienergy) bands applicable only to the Floquet operator $U(\boldsymbol{k},T)$ (or the normal part $[U(\boldsymbol{k},T)]_\varepsilon^{t/T}$). In contrast, the anomalous $U_\varepsilon(\boldsymbol{k},t)$ reduces to identity operators at $t=T$ and could be gapless at any instant $t\in(0,T)$ [84]. A completely new concept of dynamical higher-order polarization for $U_\varepsilon(\boldsymbol{k},t)$, missing in the current literature, needs to be introduced later.

As a concrete example, we check the static polarization for Eq. (1). $U(\boldsymbol{k},T)$ here possesses two quasienergy bands $\pm E_{\boldsymbol{k}}$ (see Supplemental Material [79]), each being doubly degenerate. The concise expression $E_{\boldsymbol{k}}=\arccos[\cos(\sqrt{2}\gamma)\cos(\sqrt{2}\lambda)-[(\cos k_x+\cos k_y)/2]\sin(\sqrt{2}\gamma)\sin(\sqrt{2}\lambda)]$ analytically determines the phase boundaries at $E_{\boldsymbol{k}}=0$:

$$\sqrt{2}\lambda=\pm\sqrt{2}\gamma+n\pi,\qquad n\in\mathbb{Z}. \tag{3}$$

Among the phases labeled in Fig. 2, ①–③ are normal ones with corner states fully characterized by static polarization near $x_i=1,L_x$. In particular, ① and ② are connected to high frequency limits $\gamma,\lambda\to 0$ where they reduce to the two

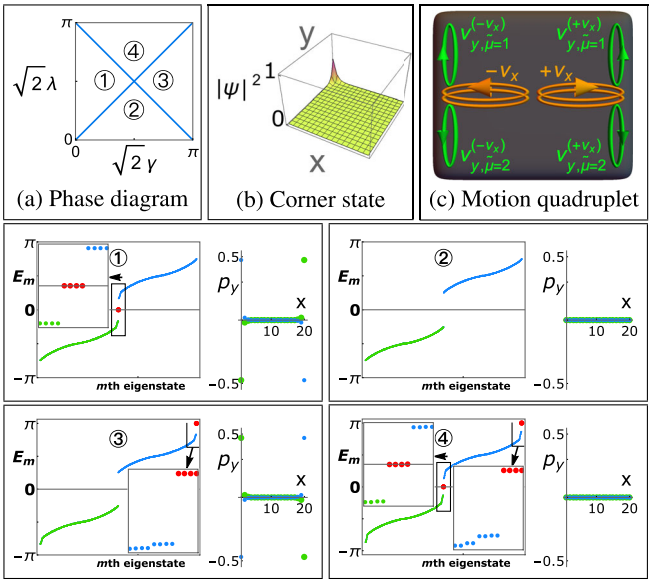

(d) Spectrum and the static polarization $p_y(x_i)$ for upper (blue) and lower (green) bands, with in-gap corner states denoted by red.

FIG. 2. (a) Phase diagram parametrized by dimensionless $(\gamma,\lambda)\equiv(\gamma' T/2\hbar,\lambda' T/2\hbar)$. (b) One representative in-gap corner state amplitude in phase ④, with others in different corners. (c) Dynamical quadrupoles beyond the description of static $p_y(x_i)$. (d) Open-boundary spectrum (left, $L_x\times L_y=20\times 20$) and static polarization in a strip periodic along y while open at $x=1,L_x$ (right, 20×100) in each panel. Parameters are $\sqrt{2}(\gamma,\lambda)=[(\pi/4),(\pi/2)],[(\pi/2),(\pi/4)],[(3\pi/4),(\pi/2)],[(\pi/2),(3\pi/4)]$ for phases ①–④.

static phases found in Ref. [35]. Contrarily, the anomalous Floquet phase ④ exhibits corner states in both gaps 0 and π well beyond the description of static polarization.

Anomalous dynamical polarization.—The absence of band physics for anomalous evolution $U_\varepsilon(\boldsymbol{k},t)$ in Eq. (2) indicates its intrinsic dynamical nature and calls for a new quantity to capture the *evolution* of polarization within $t\in[0,T]$. One naive guess would be $\hat{x}(t)=\hat{U}_\varepsilon^\dagger(t)\hat{x}\hat{U}_\varepsilon(t)$, where $\hat{U}_\varepsilon(t)\equiv\sum_{\boldsymbol{k}mn}\hat{c}^\dagger_{\boldsymbol{k}m}|0\rangle[U_\varepsilon(\boldsymbol{k},t)]_{mn}\langle 0|\hat{c}_{\boldsymbol{k}n}$ and $\hat{x}=\sum_{im}\hat{c}^\dagger_{im}|0\rangle e^{-i\Delta_x x_i}\langle 0|\hat{c}_{im}$ $(\Delta_x=2\pi/L_x, x_i=1,\ldots,L_x)$. However, $\hat{x}(t)$ turns out to possess exactly the same eigenvalues as $\hat{x}$ (see Supplemental Material [79]). Indeed, as $\hat{x}$ includes all sites, evolutions $\hat{U}_\varepsilon(t)$ to any *single* moment merely perform a gauge transformation relabeling site indices. It highlights the important lesson that dynamical polarization is to compare *relative* motion of particles at two instants, motivating the definition of dynamical mean polarization

$$\hat{x}_{\text{mean}}(t)=[\hat{x}(t)+\hat{x}(0)]/2. \tag{4}$$

To gain intuition of the newly defined quantity, we consider an idealized example. Suppose an evolution takes any site to its neighboring unit cell $x_{i+1}=x_i+1$, $\hat{U}_\varepsilon(t_0)=\sum_{im}\hat{c}^\dagger_{i+1,m}|0\rangle\langle 0|\hat{c}_{im}$. Then, $\hat{x}(t_0)=\sum_{im}\hat{c}^\dagger_{im}|0\rangle e^{-i\Delta_x(x_i+1)}\times\langle 0|\hat{c}_{im}$, which is identical to $\hat{x}(0)$ upon relabeling $\hat{c}_{im}\to\hat{c}_{i+1,m}$. In contrast, $\hat{x}_{\text{mean}}(t_0)=\sum_{im}\hat{c}^\dagger_{im}|0\rangle e^{-i\Delta_x(x_i+1/2)}\times\cos(\pi/L_x)\langle 0|\hat{c}_{im}$. The eigenvalues of $\hat{x}^{L_x}_{\text{mean}}(t_0)$ (related to dynamical Wilson loop defined later), after taking the thermodynamic limit $\lim_{L_x\to\infty}\cos^{L_x}(\pi/L_x)=1$, reads $e^{-2\pi i\nu}$ with $\nu=1/2$, giving the eigenvalues of $\hat{x}_{\text{mean}}(t_0)$ as $e^{-i\Delta_x(x_i+\nu)}$. Importantly, ν characterizes the *movement* of particles from 0 to t_0 by 2ν, rather than a static center for Wannier functions. A general proof for the unitarity of $\hat{x}_{\text{mean}}(t)$ is given in the Supplemental Material [79].

The above example illustrates the new bulk-boundary correspondence for dynamical polarization in Fig. 1(d). Since $\hat{U}_\varepsilon(T)=\hat{U}_\varepsilon(0)$ are identity operators, particles must undergo a round-trip during a cycle. But there could be nontrivial fixed point $t\in(0,T)$ where particles move by *integer* 2ν of unit cells, enforced by symmetry and topology in $\hat{U}_\varepsilon(t)$. Then, the boundary serves as obstructions for *motion*, leaving out an immobile edge or corner state. This picture differs conceptually from conventional band polarization in Fig. 1(c) where boundaries "cut" the *static* Wannier functions centering between unit cells, leaving out a decohered edge or corner state.

Rigorous constructions of dynamical polarization confirm exactly the above intuition. (See the Supplemental Material [79] for algebras). First, $\hat{x}^{L_x}_{\text{mean}}(t)=\sum_{\boldsymbol{k}mn}\hat{c}^\dagger_{\boldsymbol{k}m}|0\rangle[W_{x,\boldsymbol{k}}(t)]_{mn}\langle 0|\hat{c}_{\boldsymbol{k}n}$, where the dynamical Wilson loop at $L_x\to\infty$ reads

$$W_{x,\boldsymbol{k}}(t)=P_{k'_x}e^{-\frac{1}{2}\int_k^{k+2\pi\boldsymbol{e}_x}dk'_x U^\dagger_\varepsilon(\boldsymbol{k}',t)\partial_{k'_x}U_\varepsilon(\boldsymbol{k}',t)}, \tag{5}$$

$P_{k'_x}$ being path ordering. Diagonalizing $[W_{x,\boldsymbol{k}}(t)]_{mn}=\sum_\mu[\nu_{x,\mu}(\boldsymbol{k},t)]_m e^{-2\pi i\nu_{x,\mu}(k_y,t)}[\nu_{x,\mu}(\boldsymbol{k},t)]^*_n$, one obtains the dynamical branches μ for motions along x: $\hat{x}_{\text{mean}}(t)|b_{x,\mu}(x_i,k_y,t)\rangle=e^{-i\Delta_x(x_i+\nu_{x,\mu}(k_y,t))}|b_{x,\mu}(x_i,k_y,t)\rangle$. Crucially, the branch eigenstates $|b_{x,\mu}(x_i,k_y,t)\rangle$ should not be confused with static "edge Wannier bands" nonexistent for $U_\varepsilon(\boldsymbol{k},t)$. Instead, it represents the interference pattern of polarization at two different moments, characterizing collective motions of particles from 0 to t. This is also underscored by the number of dynamical branches μ's which *equals* sublattice numbers (i.e., four in our case), as different sublattices (or their linear combinations) can support independent Bloch-wave motions. It differs from static edge Wannier bands that halves the sublattice number due to projection onto occupied bands [35], and such a difference plays vital roles in all following analyses.

Marching toward higher orders, we group the branches μ's into sets ν_x's, where $\nu_{x,\mu_1}(k_y,t)\neq\nu_{x,\mu_2}(k_y,t)$ for μ_1,μ_2 in different ν_x's. Each set ν_x then defines a separable motion along x. The second-order dynamical polarization describes perpendicular motions within each ν_x, $\hat{y}^{(\nu_x)}_{\text{mean}}(t)\equiv\hat{P}_{\nu_x}(t)\hat{y}_{\text{mean}}(t)\hat{P}_{\nu_x}(t)$, where branch set projectors $\hat{P}_{\nu_x}(t)=\sum_{x_i,k_y,\mu\in\nu_x}|b_{x,\mu}(x_i,k_y,t)\rangle\langle b_{x,\mu}(x_i,k_y,t)|$, and $\hat{y}_{\text{mean}}(t)$ takes the form as Eq. (4) with $x\to y$. Now, $(\hat{y}^{(\nu_x)}_{\text{mean}}(t))^{L_y}$ involves nested dynamical Wilson loops (at $L_y\to\infty$) [79],

$$W^{(\nu_x)}_{y,\boldsymbol{k}}(t)=P_{k'_y}e^{-\int_k^{k+2\pi\boldsymbol{e}_y}dk'_y A^{(\nu_x)}_{y,k'}(t)}, \tag{6}$$

where the non-Abelian Berry curvature $[A^{(\nu_x)}_{y,\boldsymbol{k}}(t)]_{\mu_1\mu_2}=\sum_{mn}\frac{1}{2}[\nu_{x,\mu_1}(\boldsymbol{k},t)]^*_m[U^\dagger_\varepsilon(\boldsymbol{k},t)\partial_{k_y}U_\varepsilon(\boldsymbol{k},t)]_{mn}[\nu_{x,\mu_2}(\boldsymbol{k},t)]_n+\sum_m[\nu_{x,\mu_1}(\boldsymbol{k},t)]^*_m\partial_{k_y}[\nu_{x,\mu_2}(\boldsymbol{k},t)]_m$. Eigenvalues of $W^{(\nu_x)}_{y,\boldsymbol{k}}(t)$, $e^{-2\pi i\nu^{(\nu_x)}_{y,\tilde{\mu}}(k_x,t)}$ define the dynamical quadrupole branches $\tilde{\mu}$'s as $\nu^{(\nu_x)}_{y,\tilde{\mu}}(k_x,t)$ describes the comovement along y within the first-order branch set ν_x moving along x. See the Supplemental Material [79] for generalization to arbitrary orders in arbitrary dimensions.

Instantaneous $\nu_{x,\mu}(k_y,t)$ and $\nu^{(\nu_x)}_{y,\tilde{\mu}}(k_x,t)$ are constrained by mirror symmetries $\hat{M}_{x/y}:x/y\to-x/y$ [79]. $\hat{M}_x$ forces the four first-order branches to appear in pairs $\pm\nu_{x,\mu}(k_y,t)$, while M_y formats their shapes $\nu_{x,\mu}(k_y,t)=\nu_{x,\mu}(-k_y,t)$. Such constraints allow for the separable sets $\mu=1$, $2\in+\nu_x$, $\mu=3,4\in-\nu_x$ for our model as exemplified in Fig. 3(a). Vitally, each set contains two degenerate branches, which means the nested dynamical Wilson loops are SU(2) matrices rather than U(1) numbers in static situation [35]. $\hat{M}_x$ then dictates $\nu^{(+\nu_x)}_{y,\tilde{\mu}}(k_x,t)=\nu^{(-\nu_x)}_{y,\tilde{\mu}}(k_x,t)$ (so checking $+\nu_x$ is enough), while $\hat{M}_y$ further ensures $\nu^{(+\nu_x)}_{y,\tilde{\mu}=1}(k_x,t)=-\nu^{(+\nu_x)}_{y,\tilde{\mu}=2}(k_x,t)$ (so they can only meet at

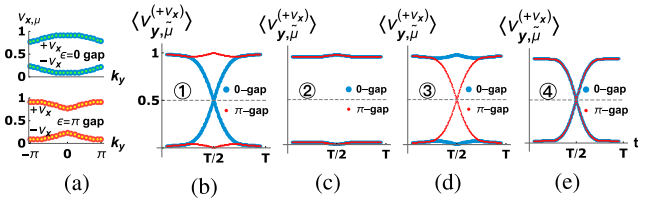

FIG. 3. (a) Exemplary first-order dynamical branches $\nu_{x,\mu}(k_y,t)$ in phase ④ at $t=T/2$. Four branches for *each* ε gap separate into two doubly degenerate sets $\pm\nu_x$. Other phases or instants t exhibit $\nu_{x,\mu}(k_y,t)$ of similar structures. (b)–(e) Quadrupolar motions $\langle\nu^{(\nu_x)}_{y,\tilde{\mu}}\rangle(t)$ in a cycle, with the same parameters as in Fig. 2 for each phase, respectively. Generically, the $1/2$ crossing needs not to occur at $t=T/2$.

$0,1/2$ mod 1). Recall that $\nu_{x,\mu}(k_y,t)$ [or $\nu^{(\nu_x)}_{y,\tilde{\mu}}(k_x,t)$] implies motions along x (or y); those constraints translate into the intuition of identical motion quadruplet along $\pm\boldsymbol{e}_x\pm\boldsymbol{e}_y$, respectively, as shown in Fig. 2(c).

Notably, *instantaneous* quadrupole branches $\nu^{(+\nu_x)}_{y,\tilde{\mu}=1,2}(k_y,t)$'s are not quantized unlike static quadrupoles [35]. True dynamical topology hides in the *evolution* of averaged quadrupolar motions $\langle\nu^{(+\nu_x)}_{y,\tilde{\mu}}\rangle(t)=\int_{-\pi}^{\pi}(dk_x/2\pi)\nu^{(+\nu_x)}_{y,\tilde{\mu}}(k_x,t)$ as shown in Fig. 3. A nontrivial evolution goes from $\langle\nu^{(+\nu_x)}_{y,\tilde{\mu}}\rangle(t\to0)=0$ to $\langle\nu^{(+\nu_x)}_{y,\tilde{\mu}}\rangle(t\to T)=1$, or vice versa, such as for the $\varepsilon=0$ gap of phase ①. Then, the two branches meeting at $1/2$ (mod 1) for $t\in(0,T)$ exactly means particles move from y_i to $y_i\pm1$ [Fig. 1(d) at "halfway"]. Because of the indistinguishability of particles, the net polarization in the open-boundary sample is from $y_i=1$ (or L_y) all the way to $y_i=L_y$ (or 1) with motions obstructed there, resulting in corner states at $y_i=1,L_y$ ($x_i=L_x$ for the $+\nu_x$ branch set). Note the two branches, or corner states at $y_i=1,L_y$, are related by $\hat{M}_y$ (see Supplemental Material [79] for mathematical meaning). Spatial separation and mirror symmetry then protect the corner states or the $1/2$ crossing for $\langle\nu^{(+\nu_x)}_{y,\tilde{\mu}=1,2}\rangle(t)$ against hybridization, leading to quantized dynamical quadrupole

$$\tilde{P}^{(+\nu_x)}_{xy,\tilde{\mu}}=\int_0^T dt(\partial_t\langle\nu^{(+\nu_x)}_{y,\tilde{\mu}}\rangle(t))\pmod 1=0,1\in\mathbb{Z}_2,\qquad(7)$$

with 1 being topologically nontrivial. Should the winding number $\tilde{P}^{(+\nu_x)}_{xy,\tilde{\mu}}=2$, the two $\langle\nu^{(+\nu_x)}_{y,\tilde{\mu}=1,2}\rangle(t_0)$ would cross at 0 mod 1 at certain $t_0\neq0,T$, which is not a stably quantized instant and $\langle\nu^{(+\nu_x)}_{y,\tilde{\mu}}\rangle(t_0)$ can be perturbed away from 0,1. Then, $\tilde{P}^{(+\nu_x)}_{xy,\tilde{\mu}}=0$ again, reducing winding numbers $\tilde{P}^{(+\nu_x)}_{xy,\tilde{\mu}}$ from $\mathbb{Z}$ to $\mathbb{Z}_2$. Physically, it means two particles polarized to the same corner can surely hybridize and gap out each other.

$\langle\nu^{(+\nu_x)}_{y,\tilde{\mu}}\rangle(t)$ for phases in Fig. 2 are shown in Figs. 3(b)–3(e), which undoubtedly capture both normal and anomalous corner states. The difference between dynamical quadrupoles in two gaps $\varepsilon=0,\pi$ gives the static quadrupole of the band sandwiched by the gaps, explaining the vanishing of static quadrupoles in phase ④.

Two remarks are in order. First, only mirror symmetries are required. In the Supplemental Material [79], extended models verify the validity of dynamical polarization when *all* accidental symmetries in Eq. (1) (time-reversal Θ, particle-hole Γ, chiral S, and fourfold rotations) are violated. In contrast, breaking mirror symmetries immediately destroys the corner states together with $\langle\nu^{(+\nu_x)}_{y,\tilde{\mu}}\rangle(t)=1/2$. Second, with only one mirror symmetry, i.e., $\hat{M}_y$, indices for our main model will change to $\mathbb{Z}$ because the sets $\pm\nu_x$ then could move in the same direction along x, each contributing a $\mathbb{Z}_2$ type of corner state adding up to $\mathbb{Z}$. In that case [46], classification for $(d+1)$-dimensional second-order insulators is completely the same as d-dimensional first-order ones determined by Θ, Γ, S, unlike ours.

Scheme for detection.—Static Hamiltonians exactly as Eq. (1) have *already* been engineered in photonic, phononic, or electric circuit experiments [38–40], which are also platforms for earlier realizations of first-order anomalous Floquet insulators driven in the form of bond connectivity [16–18]. Furthermore, experiments realizing Abelian or non-Abelian synthetic gauge fields by shaking or Raman scheme have been abundant for cold atoms [23,85–87], with the π-flux model one of the earliest prototypes [88]. For completeness, we also discussed a specific lattice quench scheme in the Supplemental Material [79]. Thus, engineering our model in diverse ranges of platforms appears immediate and we focus chiefly on detections.

First, with the digital mirror devices achieving chemical potential engineering with single-site accuracy [33], one could detect localized corner states via initially injecting particles around a potential barrier $V(x,y)=V_0\Theta(-x)\Theta(-y)$ and observing the particle density evolution, as shown in Figs. 4(a)–4(e). "Softer" corners with more smeared out potentials (a possible outcome of lattice shaking) is considered in the Supplemental Material [79], which do not affect the qualitative features as expected.

A more challenging task is to prove the triviality of Floquet operators $U(\boldsymbol{k},T)$ and confirm the dynamical origin for corner states. Our model possesses the appealing feature that parameters $\sqrt{2}\lambda$ and $\pi+\sqrt{2}\lambda$ give exactly the same $U(\boldsymbol{k},T)$ [79]. That means one can populate a certain Floquet band of phase ④ by preparing the system in static limit $\lambda\to0$, and then quench to $\lambda\to\pi/\sqrt{2}$ while maintaining band populations. (Reversed processes can be used before band mapping to determine band populations). Further, in both limits the system exhibits flat bands $\pm E_{\boldsymbol{k}}=\pm\sqrt{2}\gamma$, ideal for populating certain Floquet band homogeneously by high-temperature gases [25,26,86].

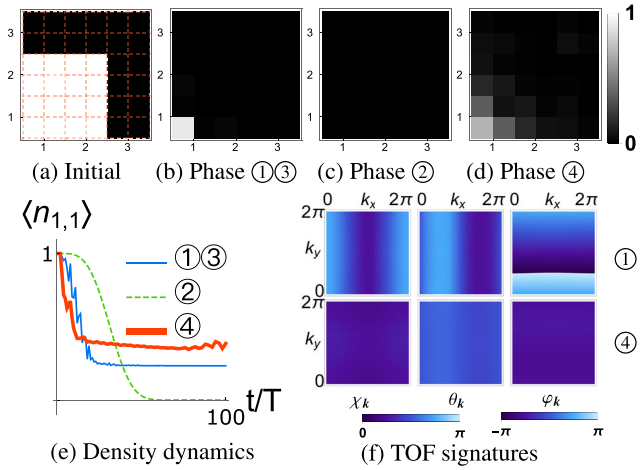

FIG. 4. Simulation of detection signatures. (a)–(d) Density evolution from (a) $t = 0$ to (b)–(d) $t = 100T$ in 20×20 unit cells (1600 sites). Only the corner 3×3 cells are shown. Each pixel denotes one lattice site, and axis ticks denote unit cells. (e) Average particle density in the unit cell $(x, y) = (1, 1)$. (f) The TOF signature for $\chi_{\boldsymbol{k}}$ (left), $\theta_{\boldsymbol{k}}$ (middle), and $\varphi_{\boldsymbol{k}}$ (right) in phase ① (upper row) and phase ④ (lower row). Parameters $(\sqrt{2}/\pi)(\gamma, \lambda) = (0.5, 0.1), (0.5, 0.05), (0.9, 0.5), (0.5, 0.95)$ for ①–④, respectively.

Then, one could perform a similar tomography experiment previously carried out in two-band static cases [24,25].

Specifically, $U(\boldsymbol{k}, T)$ for our model are parametrized by three angles $\chi_{\boldsymbol{k}}, \theta_{\boldsymbol{k}} \in [0, \pi], \varphi_{\boldsymbol{k}} \in (-\pi, \pi]$ in S^3. After equilibration, the lattice depth is ramped up and the system evolves under static chemical potentials μ_m for sublattices $m = 1$–4; three profiles of $\{\mu_i\}$ could fully determine $(\chi_{\boldsymbol{k}}, \theta_{\boldsymbol{k}}, \varphi_{\boldsymbol{k}})$ [89]. Finally, momentum density $n_{\boldsymbol{k}}$ is measured after time of flight through real-space density $n(\boldsymbol{r} = \hbar \boldsymbol{k} t/m)$. It is clear from Fig. 4(f) that the weak momentum dependence of all angles in phase ④ signals the vanishing static quadrupoles.

Conclusion.—A dynamical polarization theory is formulated here with a whole new spectrum of concepts and techniques. The central quantity, dynamical mean polarization $\hat{x}_{\text{mean}}(t)$ in Eq. (4), depicts the *temporal* interference pattern for Bloch-wave evolutions. It serves as a natural and qualitative generalization of static polarization (corresponding to $\hat{y}_{\text{occ}}$) characterizing *spatial* interference patterns for Bloch waves of occupied bands in different sublattices. Validity of dynamical polarization theory in Eqs. (5) and (6) transcends specific dimensions and/or symmetries, offering a generic way to define and study dynamical multipoles in driven or quenched systems. The first proposal to unambiguously detect the anomalous character of Floquet phases beyond band descriptions is also provided.

This work is supported by the Air Force Office of Scientific Research (Grant No. FA9550-16-1-0006), Multidisciplinary University Research Initiative program through Army Research Office (Grant No. W911NF-17-1-0323), and Shanghai Municipal Science and Technology Major Project (Grant No. 2019SHZDZX01).

Note added.—Recently, we noted two preprints [90,91] constructing model- or symmetry-dependent topological invariants, and another on classification with a single mirror symmetry [92]. Also, there appeared a complementary proposal [93] to measure first-order Floquet topology. Normal Floquet phases are explored more in Ref. [94].

*phys.huang.biao@gmail.com
†wvliu@pitt.edu

[1] V. Khemani, A. Lazarides, R. Moessner, and S. L. Sondhi, Phys. Rev. Lett. **116**, 250401 (2016).
[2] D. V. Else, B. Bauer, and C. Nayak, Phys. Rev. Lett. **117**, 090402 (2016).
[3] N. Y. Yao, A. C. Potter, I.-D. Potirniche, and A. Vishwanath, Phys. Rev. Lett. **118**, 030401 (2017).
[4] J. Zhang, P. Hess, A. Kyprianidis, P. Becker, A. Lee, J. Smith, G. Pagano, I.-D. Potirniche, A. C. Potter, A. Vishwanath *et al.*, Nature (London) **543**, 217 (2017).
[5] S. Choi, J. Choi, R. Landig, G. Kucsko, H. Zhou, J. Isoya, F. Jelezko, S. Onoda, H. Sumiya, V. Khemani *et al.*, Nature (London) **543**, 221 (2017).
[6] J. Rovny, R. L. Blum, and S. E. Barrett, Phys. Rev. Lett. **120**, 180603 (2018).
[7] K. Sacha, Phys. Rev. A **91**, 033617 (2015).
[8] W. W. Ho, S. Choi, M. D. Lukin, and D. A. Abanin, Phys. Rev. Lett. **119**, 010602 (2017).
[9] B. Huang, Y.-H. Wu, and W. V. Liu, Phys. Rev. Lett. **120**, 110603 (2018).
[10] K. Sacha and J. Zakrzewski, Rep. Prog. Phys. **81**, 016401 (2018).
[11] N. Yao and C. Nayak, Phys. Today **71**, No. 9, 40 (2018) .
[12] C. W. von Keyserlingk, V. Khemani, and S. L. Sondhi, Phys. Rev. B **94**, 085112 (2016).
[13] M. S. Rudner, N. H. Lindner, E. Berg, and M. Levin, Phys. Rev. X **3**, 031005 (2013).
[14] R. Roy and F. Harper, Phys. Rev. B **96**, 155118 (2017).
[15] S. Yao, Z. Yan, and Z. Wang, Phys. Rev. B **96**, 195303 (2017).
[16] S. Mukherjee, A. Spracklen, M. Valiente, E. Andersson, P. Öhberg, N. Goldman, and R. R. Thomson, Nat. Commun. **8**, 13918 (2017).
[17] Y.-G. Peng, C.-Z. Qin, D.-G. Zhao, Y.-X. Shen, X.-Y. Xu, M. Bao, H. Jia, and X.-F. Zhu, Nat. Commun. **7**, 13368 (2016).
[18] L. J. Maczewsky, J. M. Zeuner, S. Nolte, and A. Szameit, Nat. Commun. **8**, 13756 (2016).
[19] C. W. von Keyserlingk and S. L. Sondhi, Phys. Rev. B **93**, 245145 (2016).
[20] D. V. Else and C. Nayak, Phys. Rev. B **93**, 201103(R) (2016).
[21] I.-D. Potirniche, A. C. Potter, M. Schleier-Smith, A. Vishwanath, and N. Y. Yao, Phys. Rev. Lett. **119**, 123601 (2017).

[22] A. Eckardt, Rev. Mod. Phys. **89**, 011004 (2017).
[23] N. R. Cooper, J. Dalibard, and I. B. Spielman, Rev. Mod. Phys. **91**, 015005 (2019).
[24] P. Hauke, M. Lewenstein, and A. Eckardt, Phys. Rev. Lett. **113**, 045303 (2014).
[25] N. Fläschner, B. Rem, M. Tarnowski, D. Vogel, D.-S. Lühmann, K. Sengstock, and C. Weitenberg, Science **352**, 1091 (2016).
[26] T. Li, L. Duca, M. Reitter, F. Grusdt, E. Demler, M. Endres, M. Schleier-Smith, I. Bloch, and U. Schneider, Science **352**, 1094 (2016).
[27] N. Fläschner, D. Vogel, M. Tarnowski, B. Rem, D.-S. Lühmann, M. Heyl, J. Budich, L. Mathey, K. Sengstock, and C. Weitenberg, Nat. Phys. **14**, 265 (2018).
[28] W. Sun, C.-R. Yi, B.-Z. Wang, W.-W. Zhang, B. C. Sanders, X.-T. Xu, Z.-Y. Wang, J. Schmiedmayer, Y. Deng, X.-J. Liu, S. Chen, and J.-W. Pan, Phys. Rev. Lett. **121**, 250403 (2018).
[29] C. Wang, P. Zhang, X. Chen, J. Yu, and H. Zhai, Phys. Rev. Lett. **118**, 185701 (2017).
[30] L. Zhang, L. Zhang, and X.-J. Liu, Phys. Rev. A **99**, 053606 (2019).
[31] M. Endres, H. Bernien, A. Keesling, H. Levine, E. R. Anschuetz, A. Krajenbrink, C. Senko, V. Vuletic, M. Greiner, and M. D. Lukin, Science **354**, 1024 (2016).
[32] A. Mazurenko, C. S. Chiu, G. Ji, M. F. Parsons, M. Kanász-Nagy, R. Schmidt, F. Grusdt, E. Demler, D. Greif, and M. Greiner, Nature (London) **545**, 462 (2017).
[33] M. E. Tai, A. Lukin, M. Rispoli, R. Schittko, T. Menke, D. Borgnia, P. M. Preiss, F. Grusdt, A. M. Kaufman, and M. Greiner, Nature (London) **546**, 519 (2017).
[34] P. T. Brown, D. Mitra, E. Guardado-Sanchez, R. Nourafkan, A. Reymbaut, S. Bergeron, A. M. S. Tremblay, J. Kokalj, D. A. Huse, P. Schauss, and W. S. Bakr, Science **363**, 379 (2018).
[35] W. A. Benalcazar, B. A. Bernevig, and T. L. Hughes, Science **357**, 61 (2017).
[36] W. A. Benalcazar, B. A. Bernevig, and T. L. Hughes, Phys. Rev. B **96**, 245115 (2017).
[37] J. Noh, W. A. Benalcazar, S. Huang, M. J. Collins, K. P. Chen, T. L. Hughes, and M. C. Rechtsman, Nat. Photonics **12**, 408 (2018).
[38] M. Serra-Garcia, V. Peri, R. Süsstrunk, O. R. Bilal, T. Larsen, L. G. Villanueva, and S. D. Huber, Nature (London) **555**, 342 (2018).
[39] C. W. Peterson, W. A. Benalcazar, T. L. Hughes, and G. Bahl, Nature (London) **555**, 346 (2018).
[40] S. Imhof, C. Berger, F. Bayer, J. Brehm, L. Molenkamp, T. Kiessling, F. Schindler, C. H. Lee, M. Greiter, T. Neupert, and R. Thomale, Nat. Phys. **14**, 925 (2018).
[41] Z. Wang, B. J. Wieder, J. Li, B. Yan, and B. A. Bernevig, Phys. Rev. Lett. **123**, 186401 (2019).
[42] F. Schindler, Z. Wang, M. G. Vergniory, A. M. Cook, A. Murani, S. Sengupta, A. Y. Kasumov, R. Deblock, S. Jeon, I. Drozdov, H. Bouchiat, S. Guéron, A. Yazdani, B. A. Bernevig, and T. Neupert, Nat. Phys. **14**, 918 (2018).
[43] F. K. Kunst, G. van Miert, and E. J. Bergholtz, Phys. Rev. B **97**, 241405(R) (2018).
[44] F. Schindler, A. M. Cook, M. G. Vergniory, Z. Wang, S. S. Parkin, B. A. Bernevig, and T. Neupert, Sci. Adv. **4**, eaat0346 (2018).
[45] Z. Song, Z. Fang, and C. Fang, Phys. Rev. Lett. **119**, 246402 (2017).
[46] J. Langbehn, Y. Peng, L. Trifunovic, F. von Oppen, and P. W. Brouwer, Phys. Rev. Lett. **119**, 246401 (2017).
[47] L. Trifunovic and P. Brouwer, Phys. Rev. X **9**, 011012 (2019).
[48] D. Calugaru, V. Juricic, and B. Roy, Phys. Rev. B **99**, 041301 (2019).
[49] R. Queiroz and A. Stern, Phys. Rev. Lett. **123**, 036802 (2019).
[50] M. Ezawa, Phys. Rev. Lett. **121**, 116801 (2018).
[51] M. Lin and T. L. Hughes, Phys. Rev. B **98**, 241103 (2018).
[52] M. Ezawa, Phys. Rev. Lett. **120**, 026801 (2018).
[53] M. Ezawa, Phys. Rev. B **97**, 155305 (2018).
[54] H. Shapourian, Y. Wang, and S. Ryu, Phys. Rev. B **97**, 094508 (2018).
[55] Y. Wang, M. Lin, and T. L. Hughes, Phys. Rev. B **98**, 165144 (2018).
[56] E. Khalaf, Phys. Rev. B **97**, 205136 (2018).
[57] X. Zhu, Phys. Rev. B **97**, 205134 (2018).
[58] Z. Yan, F. Song, and Z. Wang, Phys. Rev. Lett. **121**, 096803 (2018).
[59] Q. Wang, C.-C. Liu, Y.-M. Lu, and F. Zhang, Phys. Rev. Lett. **121**, 186801 (2018).
[60] T. Liu, J. J. He, and F. Nori, Phys. Rev. B **98**, 245413 (2018).
[61] V. Dwivedi, C. Hickey, T. Eschmann, and S. Trebst, Phys. Rev. B **98**, 054432 (2018).
[62] Y. You, T. Devakul, F. J. Burnell, and T. Neupert, Phys. Rev. B **98**, 235102 (2018).
[63] A. Rasmussen and Y.-M. Lu, Phys. Rev. B **101**, 085137 (2020).
[64] See also earlier related works [95,96].
[65] H. C. Po, L. Fidkowski, A. Vishwanath, and A. C. Potter, Phys. Rev. B **96**, 245116 (2017).
[66] K. Hashimoto, S. Kinoshita, K. Murata, and T. Oka, J. High Energy Phys. (2017) 127.
[67] S. Kinoshita, K. Murata, and T. Oka, J. High Energy Phys. (2018) 096.
[68] T. Ishii and K. Murata, Phys. Rev. D **98**, 126005 (2018).
[69] P. Titum, E. Berg, M. S. Rudner, G. Refael, and N. H. Lindner, Phys. Rev. X **6**, 021013 (2016).
[70] A. C. Potter, T. Morimoto, and A. Vishwanath, Phys. Rev. X **6**, 041001 (2016).
[71] L. Fidkowski, H. C. Po, A. C. Potter, and A. Vishwanath, Phys. Rev. B **99**, 085115 (2019).
[72] J. Shapiro and C. Tauber, arXiv:1807.03251.
[73] D. Reiss, F. Harper, and R. Roy, Phys. Rev. B **98**, 045127 (2018).
[74] D. E. Liu, A. Levchenko, and H. U. Baranger, Phys. Rev. Lett. **111**, 047002 (2013).
[75] M. Thakurathi, D. Loss, and J. Klinovaja, Phys. Rev. B **95**, 155407 (2017).
[76] B. Bauer, T. Pereg-Barnea, T. Karzig, M.-T. Rieder, G. Refael, E. Berg, and Y. Oreg, Phys. Rev. B **100**, 041102 (2019).
[77] The direct product of Pauli matrices $\boldsymbol{\tau}, \boldsymbol{\sigma}$ can be understood as, i.e., $\tau_3\sigma_1 = \left(\begin{smallmatrix}\sigma_1 & 0\\ 0 & -\sigma_1\end{smallmatrix}\right)$.
[78] R. Resta, Phys. Rev. Lett. **80**, 1800 (1998).
[79] See Supplemental Material at http://link.aps.org/supplemental/10.1103/PhysRevLett.124.216601 for algebras of dynamical polarization theory, analytical expressions

for Floquet spectrum and periodized evolution operator, numerical algorithm, and more details for experimental proposals. It includes additional Refs. [80–83].

[80] H.-N. Dai, B. Yang, A. Reingruber, X.-F. Xu, X. Jiang, Y.-A. Chen, Z.-S. Yuan, and J.-W. Pan, Nat. Phys. **12**, 783 (2016).

[81] X.-J. Liu, M. F. Borunda, X. Liu, and J. Sinova, Phys. Rev. Lett. **102**, 046402 (2009).

[82] M. Aidelsburger, M. Atala, S. Nascimbène, S. Trotzky, Y.-A. Chen, and I. Bloch, Phys. Rev. Lett. **107**, 255301 (2011).

[83] M. Tarnowski, M. Nuske, N. Fläschner, B. Rem, D. Vogel, L. Freystatzky, K. Sengstock, L. Mathey, and C. Weitenberg, Phys. Rev. Lett. **118**, 240403 (2017).

[84] In fact, $U_\varepsilon(\boldsymbol{k}, t)$ being gapless at certain $(\boldsymbol{k}, t)$ leads to the well-known concept of "dynamical singularity" [97].

[85] L. Duca, T. Li, M. Reitter, I. Bloch, M. Schleier-Smith, and U. Schneider, Science **347**, 288 (2015).

[86] M. Aidelsburger, M. Lohse, C. Schweizer, M. Atala, J. T. Barreiro, S. Nascimbene, N. Cooper, I. Bloch, and N. Goldman, Nat. Phys. **11**, 162 (2015).

[87] Z. Wu, L. Zhang, W. Sun, X.-T. Xu, B.-Z. Wang, S.-C. Ji, Y. Deng, S. Chen, X.-J. Liu, and J.-W. Pan, Science **354**, 83 (2016).

[88] M. Aidelsburger, M. Atala, M. Lohse, J. T. Barreiro, B. Paredes, and I. Bloch, Phys. Rev. Lett. **111**, 185301 (2013).

[89] There are infinitely many choices to back up the angles. We demonstrate one such choice in the Supplemental Material [79].

[90] R. W. Bomantara, L. Zhou, J. Pan, and J. Gong, Phys. Rev. B **99**, 045441 (2019).

[91] M. Rodriguez-Vega, A. Kumar, and B. Seradjeh, Phys. Rev. B **100**, 085138 (2019).

[92] Y. Peng and G. Refael, Phys. Rev. Lett. **123**, 016806 (2019).

[93] F. N. Ünal, B. Seradjeh, and A. Eckardt, Phys. Rev. Lett. **122**, 253601 (2019).

[94] R. Seshadri, A. Dutta, and D. Sen, Phys. Rev. B **100**, 115403 (2019).

[95] F. Zhang, C. L. Kane, and E. J. Mele, Phys. Rev. Lett. **110**, 046404 (2013).

[96] B. Seradjeh, C. Weeks, and M. Franz, Phys. Rev. B **77**, 033104 (2008).

[97] F. Nathan and M. S. Rudner, New J. Phys. **17**, 125014 (2015).